ACS NANO

www.acsnano.org

ARTICLE

Self-Powered Acceleration Sensor Based on Liquid Metal Triboelectric Nanogenerator for Vibration Monitoring

Binbin Zhang,[†,⊥] Lei Zhang,[†,⊥] Weili Deng,[†] Long Jin,[†] Fengjun Chun,[†] Hong Pan,[†] Bingni Gu,[†] Haitao Zhang,[†] Zekai Lv,[†] Weiqing Yang,[*,†,§] and Zhong Lin Wang[*,‡,∥]

[†]Key Laboratory of Advanced Technologies of Materials (Ministry of Education), School of Materials Science and Engineering and [§]State Key Laboratory of Traction Power, Southwest Jiaotong University, Chengdu 610031, China

[‡]School of Materials Science and Engineering, Georgia Institute of Technology, Atlanta, Georgia 30332, United States

[∥]Beijing Institute of Nanoenergy and Nanosystems, Chinese Academy of Sciences, Beijing 100083, China

Supporting Information

ABSTRACT: **An acceleration sensor is an essential component of the vibration measurement, while the passivity and sensitivity are the pivotal features for its application. Here, we report a self-powered and highly sensitive acceleration sensor based on a triboelectric nanogenerator composed of a liquid metal mercury droplet (LMMD) and nanofiber-networked polyvinylidene fluoride (nn-PVDF) film. Due to the ultrahigh surface-to-volume ratio of nn-PVDF film and high surface tension, high mass density, high elastic as well as mechanical robustness of LMMD, the open-circuit voltage and short-circuit current reach up to 15.5 V and 300 nA at the acceleration of 60 m/s^2, respectively. The acceleration sensor has a wide detection range from 0 to 60 m/s^2 with a high sensitivity of 0.26 V·s/m^2. Also, the output voltage and current show a negligible decrease over 200,000 cycles, evidently presenting excellent stability. Moreover, a high-speed camera was employed to dynamically capture the motion state of the acceleration sensor for insight into the corresponding work mechanism. Finally, the acceleration sensor was demonstrated to measure the vibration of mechanical equipment and human motion in real time, which has potential applications in equipment vibration monitoring and troubleshooting.**

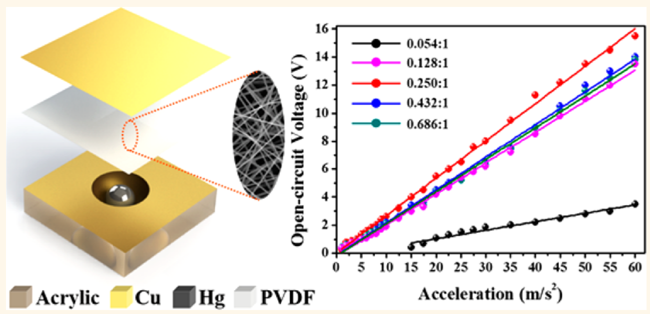

KEYWORDS: *self-powered, acceleration sensor, liquid metal, triboelectric nanogenerator, vibration monitoring*

An acceleration sensor is a critical component in vibration monitoring, which acts a pivotal part in many fields such as global position system, biomedical devices, intelligent electronic products, vehicle safety, earthquake monitoring, and mechanical equipment vibration monitoring and troubleshooting.[1,2] Usually, the acceleration sensor can be generally classified into piezoelectric, capacitive, and piezoresistive types,[3] among which the piezoelectric sensor is self-powered, while the electric output is very small and could be influenced by the environmental noise.[4] Moreover, the capacitive and piezoresistive acceleration sensors are mainly powered by the traditional power supply unit, which will limit their potential applications.[5] Hence, it is highly desired to fabricate an acceleration sensor with a large output signal and the ability to be self-powered simultaneously.

Recently, the triboelectric nanogenerator (TENG) has been proved to be a robust way to convert ambient mechanical energy into electric energy due to a coupling effect of contact electrification and electrostatic induction.[6−11] Ascribing to the outstanding properties such as high performance, high conversion efficiency, easy fabrication, low cost, and easy scalability, TENG has been utilized to harvest the energy produced by the wind,[12,13] water wave,[14−16] human walking,[17,18] and so on. More importantly, TENG can also act as self-powered sensors for actively detecting the static and dynamic processes arising from mechanical stimulation using the voltage and current output signals of the TENG, including pressure sensor,[19] vibration sensor,[20] traffic volume sensor,[21] motion sensor,[22] angle sensor,[23,24] tactile sensor,[25] biosensor,[26] acoustic sensor,[27] velocity sensor,[28] and so on. However, only a few papers explored the process of utilizing a TENG to detect

Received: May 31, 2017
Accepted: July 3, 2017
Published: July 3, 2017

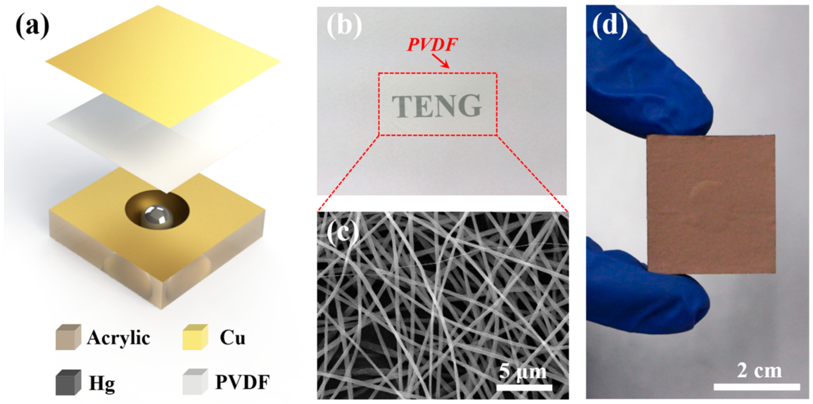

Figure 1. Structural design of the self-powered acceleration sensor. (a) Schematic diagram of the self-powered acceleration sensor for vibration monitoring. (b) Photograph of the nn-PVDF film composed of nanofibers. (c) SEM image of PVDF nanofibers. (d) Photograph of the fully assembled acceleration sensor.

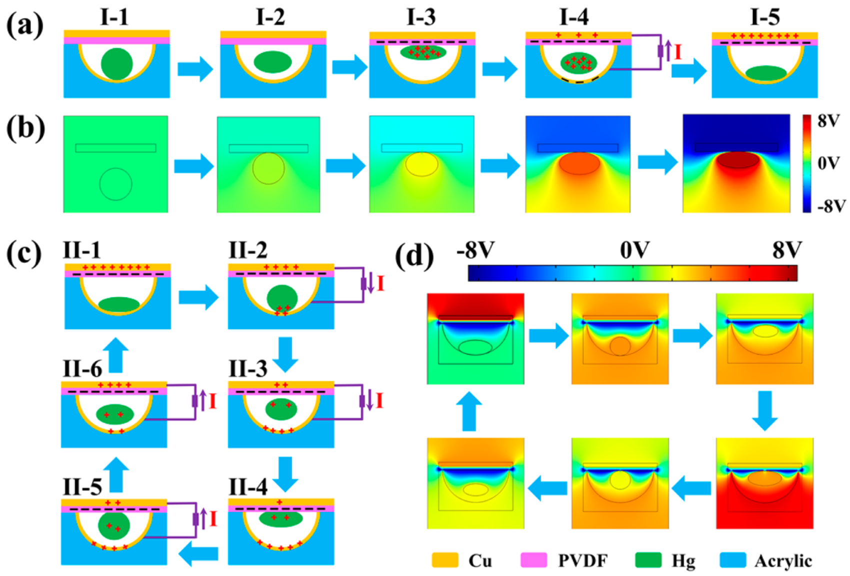

Figure 2. Theoretical investigation on the working principle of the acceleration sensor. (a) Contact electrification stage where the charge transferred at the interface of the nn-PVDF film and mercury droplet. (b) Numerical calculations on the potential differences between the nn-PVDF film and mercury droplet at the contact electrification stage. (c) Electrostatic induction stage where the charge transferred between the two copper electrodes. (d) Numerical calculations on the potential differences at electrostatic induction by COMSOL.

acceleration. Zhang *et al.* have reported a self-powered acceleration sensor which can detect the acceleration ranging from 10 m/s^2 to 20 m/s^2.[29] Pang *et al.* also have reported a 3D acceleration sensor with a detection range from 13 m/s^2 to 40 m/s^2.[1] One of the most common flaws in the above-mentioned acceleration sensors is that they cannot detect the acceleration below 10 m/s^2. In addition, the size of the sensors is too large for applications. In this regard, it is necessary to develop techniques to fabricate acceleration sensors with both small size and wide detection range.

In this work, we demonstrate a self-powered acceleration sensor based on liquid metal triboelectric nanogenerator, which was composed of an inner liquid metal droplet (mercury) and an outer acrylic shell. A nanofiber-networked polyvinylidene fluoride (nn-PVDF) film was prepared by a simple electrospinning method as one of the triboelectric layers. Ascribing to ultrahigh surface-to-volume ratio, the nanofiber structure can efficiently generate charges on its surface, which is beneficial for triboelectric power generation.[30−32] For a systematical study, a high-speed camera was employed to clearly capture the motion states and interaction between the mercury droplet and the triboelectric layers. With a device size of 30 × 30 × 6 mm, the sensor can be used to measure acceleration attributed to the linearly proportional relationship between the acceleration and the electric output, where the detection range and sensitivity are 0−60 m/s^2 and 0.26 $V \cdot s/m^2$. At the acceleration of 60 m/s^2, the open-circuit voltage and short-circuit current, respectively, reach up to 15.5 V and 300 nA. The output voltage and current show a negligible decrease over 200,000 cycles, evidently presenting excellent stability. More importantly, the self-powered acceleration sensor can be used to measure the vibration of mechanical equipment and human motion in real time. This work presents solid progress toward the practical applications of triboelectric nanogenerators in vibration measurement and equipment troubleshooting techniques.

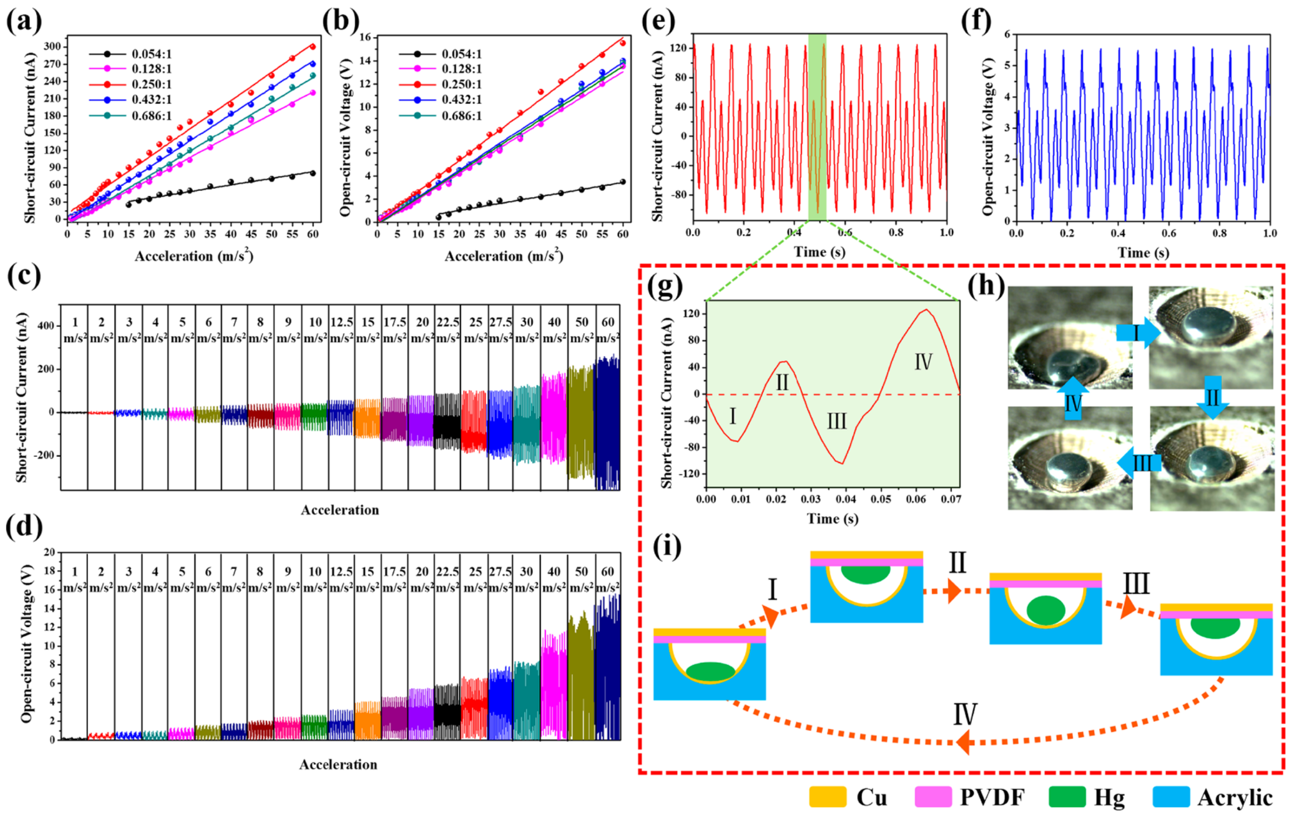

Figure 3. Electrical output performance of the acceleration sensor based on TENG. (a, b) Dependence of the short-circuit current (a) and open-circuit voltage (b) of TENG with different volume ratios of the mercury droplet and acrylic pit on accelerations ranging from 0 to 60 m/s^2. (c, d) Short-circuit current (c) and open-circuit voltage (d) of the sensor with a volume ratio of 0.25:1 at variable accelerations. (e, f) Short-circuit current (e) and open-circuit voltage (f) of the sensor with a volume ratio of 0.25:1 at the acceleration of 20 m/s^2. (g) Enlarged view of the short-circuit current in one vibration period. (h) Motion state of mercury droplet in one vibration period captured by a high-speed camera at the acceleration of 20 m/s^2. (i) Sketch diagram of the mercury droplet motion state in one vibration period.

RESULTS AND DISCUSSION

Figure 1a schematically shows the basic configuration of the self-powered acceleration sensor based on liquid metal TENG, which consists of an inner mercury droplet and an outer acrylic shell. For a typical fabrication of device, a hemisphere-shaped pit with a 10 mm diameter was sculptured on the surface of an acrylic plate by a laser cutter. A thin copper film was deposited on the acrylic surface as the electrode. Compared to other conductive solutions such as water, the liquid metal exhibits more extraordinary properties, for example, higher electric conductivity, higher mass density, higher solid−liquid interfacial tension, higher elasticity, and better mechanical robustness. The nonstick mercury droplet was placed into the pit as a floating electrode.[33,34] On the top of the pit, a layer of Cu-coated nn-PVDF was laminated as one of the triboelectric layers. The fabrication process is schematically illustrated in Supporting Figure S1. PVDF was purposely chosen according to the triboelectric series, as shown in Supporting Table S1, which can easily gain electrons from the mercury droplet. More importantly, in order to enhance the effective contact area and improve the output performance of the TENG, the electrospinning process was employed to make a nanofiber-networked PVDF film, as illustrated in Figure 1b. The schematic diagram of electrospinning process is illustrated in Supporting Figure S2. The PVDF nanofibers have a uniform size distribution and an average diameter of 290 nm, as shown in Figure 1c and Supporting Figure S3. Figure 1d is a digital photograph of the acceleration sensor with a small size of 30 × 30 × 6 mm and the low weight of 8g.

The basic working principle of the acceleration sensor is schematically plotted in Figure 2. Here, the working principle can be elucidated from two aspects: the contact electrification and the electrostatic induction process. As shown in Figure 2a, at original stage I-1, the mercury droplet stays at the bottom of the acrylic pit, and there is no electric charge on the surface of the nn-PVDF film. Once the acceleration sensor starts to move up (stage I-2), the mercury droplet will intimately contact with the nn-PVDF film (stage I-3), ascribing to the different triboelectric polarity of the PVDF and mercury, and charge transfer at the interface will make the nn-PVDF negatively charged and mercury droplet positively charged. The tribo-charges will sustain on the nn-PVDF film surface and cannot be conducted away or neutralized for an extended period of time due to the nature of the dielectric.[35−38] At this moment, triboelectric charges with opposite polarities are fully balanced out delicately, meaning no electric charge transfer between the electrodes. When the mercury separates from the nn-PVDF film surface along with the sensor moving down (stage I-4), the equilibration of electric field is changed, and then an electric potential difference is created between the copper electrodes. The electrons will flow from the top electrode to the bottom electrode until the accumulated charges reach an equilibrium state (stage I-5). COMSOL was employed to simulate the potential distribution between the mercury and nn-PVDF film upon contact and separation, as illustrated in Figure 2b and

DOI: 10.1021/acsnano.7b03818
ACS Nano XXXX, XXX, XXX−XXX

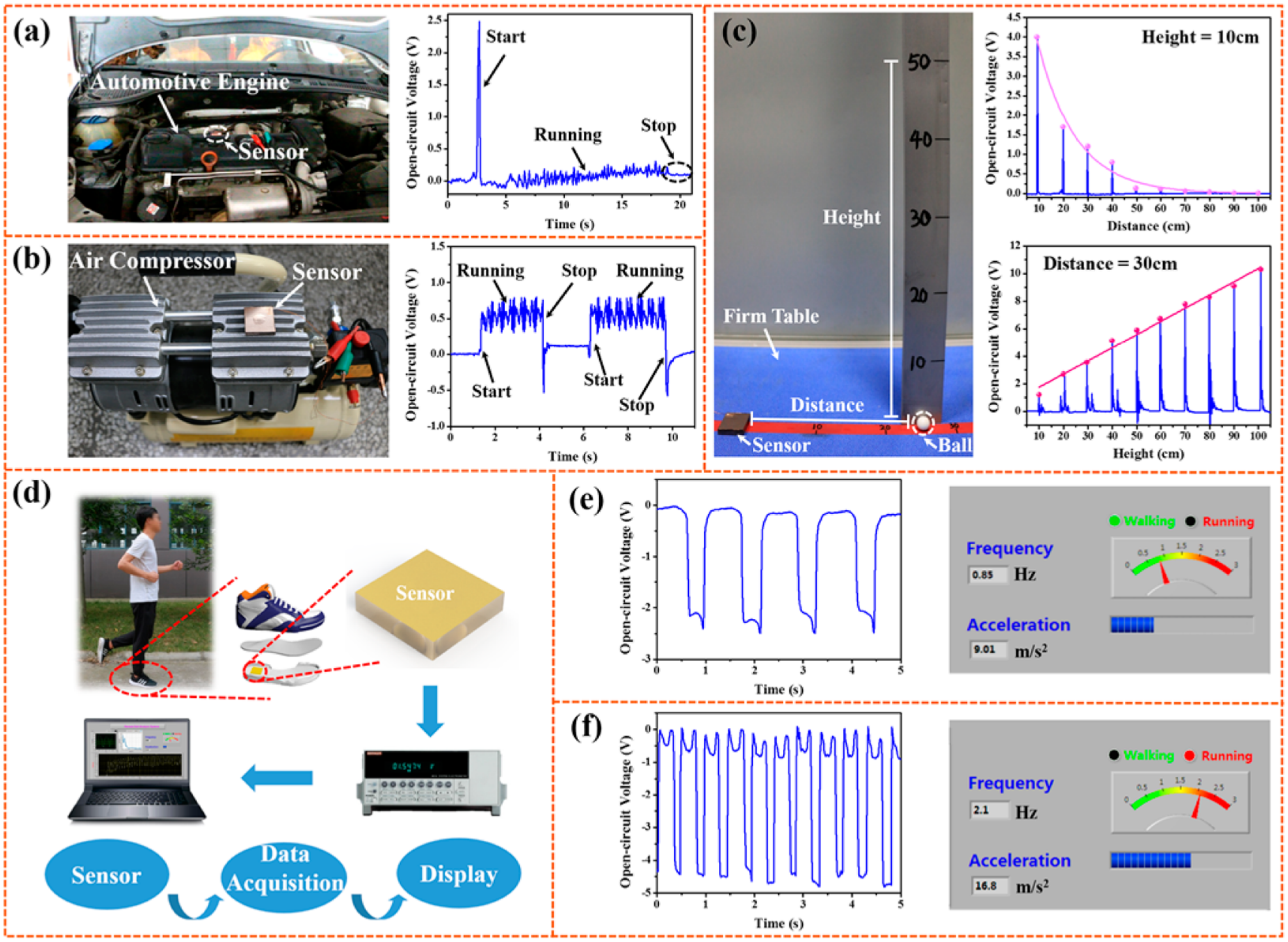

Figure 4. Demonstration of the acceleration sensor for vibration monitoring. (a, b) Acceleration sensor was fixed onto the automotive engine (a) and air compressor (b) to monitor their working state. (c) Acceleration sensor was utilized to measure the vibration of a firm table caused by the impact between a little ball and the table. (d) Schematic diagram of the self-powered human gait analysis system. (e) Gait analysis of human walking. (f) Gait analysis of human running.

Supporting Movie 1. When it comes to the electrostatic induction process, its working mechanism is clearly displayed in Figure 2c. When the acceleration sensor moves up again (stages II-2 and 3), the distance between the mercury droplet and nn-PVDF film decreases, and the potential difference starts to drop resulting in the generation of electrons flow from the bottom electrode to the top electrode. The flow of induced electrons can last until a new electrical equilibrium is established (stage II-4). Once the mercury droplet moves down (stage II-5 and 6), non-equilibrium of the potential will drive the electrons to flow from the top electrode to the bottom electrode again until to the equilibrium stage II-1. The potential distribution of nn-PVDF film and electrodes at electrostatic induction stage is calculated *via* COMSOL, as clearly illustrated in Figure 2d and Supporting Movie 2.

To characterize the performance of the acceleration sensor, the output performances of the sensor with different volume ratio of mercury droplet and acrylic pit vibrating at different accelerations were measured. The acceleration sensor was mounted on the linear motor, and the moving distance of the linear motor is fixed. With the oscillation of the linear motor, the sensor is moving up-and-down, and the acceleration can be precisely controlled by a linear motor. The open-circuit voltages and short-circuit current of the acceleration sensor with volume ratio of 0.128:1 at variable acceleration ranging from 0 to 100 m/s^2 were measured, as shown in Figure S4. The open-circuit voltage increases in the initial stage and then decreases at the larger acceleration. It is attributed to the motion state of mercury droplet, which is transformed from the up-and-down motion to rotational motion in the pit when the acceleration exceeded 60 m/s^2. It is indicated that the detection range of the acceleration sensor is 0−60 m/s^2. As shown in Figure 3a,b, both the short-circuit current and open-circuit voltage of the acceleration sensor are proportional to the external vibration acceleration in a wide range from 0 to 60 m/s^2. Moreover, the output current and voltage first offer an upgrade with increasing the diameter of mercury droplet, however, abruptly descending after the maximized volume ratio of 0.25:1. For the acceleration sensor with a volume ratio of 0.054:1, the detection range is 15−60 m/s^2, ascribing to that the mercury droplet not contact the surface of the nn-PVDF film when the acceleration is below 15 m/s^2. The short-circuit current and open-circuit voltage curves of the sensor with volume ratio of 0.25:1 at variable accelerations are shown in Figure 3c,d and reach up to 300 nA and 15.5 V under the acceleration of 60 m/s^2, respectively. It is distinctly demonstrated that the acceleration sensor not only possesses the ability to detect the vibration acceleration but also can measure the frequency. The acquired signals of the sensor with a volume ratio of 0.25:1 at variable accelerations of 1, 5, 10, 15,

DOI: 10.1021/acsnano.7b03818
ACS Nano XXXX, XXX, XXX−XXX

25, 30, 40, 50, and 60 m/s^2 are illustrated in Supporting Figures S5 and S6, when their vibration times are fixed at 5 s. It can be clearly seen that all of the output electric signals are uniform and stable. To clearly provide the valuable insight into the working mechanism of the sensor, a high-speed camera with a frame rate of 4000 Hz was employed to dynamically capture the contact-separation process between the mercury droplet and triboelectric layers, as shown in Supporting Movie 3. An interesting phenomenon was found that the mercury droplet contacts and separates with the nn-PVDF film twice during one period of linear motor moving, which can be verified by the electric output of the acceleration sensor. At an acceleration of 20 m/s^2, the frequency of open-circuit voltage and short-circuit current is 27.6 Hz, as shown in Figure 3e,f, doubling the vibration frequency (13.8 Hz) of the linear motor, which was calculated from the movie captured by high-speed camera. The detailed discussion of the vibration process is clearly demonstrated in Figure 3g−i. At stage I, when the linear motor moves from bottom to top, the mercury droplet will approach and gradually contact the surface of nn-PVDF film, resulting in an induced negative current. Whereafter, the acceleration sensor will move down along with the linear motor. In the process, the mercury droplet will first fall from the top and contact with the bottom electrode (stage II) and then immediately bounce up (stage III) and contact with the nn-PVDF film again, and finally, it will drop to the bottom of the sensor (stage IV) at the same time as the linear motor moves to the lowest point. As a result, the continuous positive, negative, and positive current is produced in the circuit. In addition, the stability test of the acceleration sensor was carried out at the acceleration of 20 m/s^2. As shown in Figure S7, after 200,000 vibration cycles, the open-circuit voltage and short-circuit current exhibit only negligible drops, indicating high durability of the acceleration sensor, ascribing to that the liquid−solid contact of mercury droplet and nn-PVDF film reduces the abrasion of nanostructures.

To prove the capability of the liquid metal TENG as an acceleration sensor for vibration measurement and analysis, four sets of practical applications were demonstrated. First, as illustrated in Figure 4a and Supporting Movie 4, the acceleration sensor was mounted onto an automotive engine and efficiently detected the operating state. The open-circuit voltage rapidly increased to 2.5 V as the car started, then dropped to nearly 0.25 V and kept until the car stopped. Similarly, the acceleration sensor also can be fixed on the mechanical equipment such as air compressor to monitor the operating state, as clearly demonstrated in Figure 4b. The third practical application shows that the acceleration sensor, mounted on a firm table, can detect the vibration of the table caused by the impact between a little ball and the table. The diameter of the little ball is 10 mm, and the weight is 10.5 g. With a falling height of 10 cm, the electric output amplitude is exponentially related to the distance between the acceleration sensor and the falling point of the ball. Moreover, when the distance between the sensor and falling point was controlled at 30 cm, the open-circuit voltage of the sensor is proportional to the falling height of the little ball, as shown in Figure 4c. At last, the acceleration sensor was embedded in the shoes for human gait analyzing in real time, as illustrated in Figure 4 d. When a human first begins to exercise, the frequency and acceleration of falling steps could be detected by the self-powered human gait analysis system. The open-circuit voltages of the acceleration sensor in the walking state and running state are enumerated in Figure 4e,f. According to the frequency and value of the output voltage, the types of human motion and acceleration of falling steps could be calculated, as shown in Supporting Movie 5. It is indicated that the self-powered acceleration sensor will greatly promote the development of vibration measurement and analysis.

CONCLUSION

In summary, we have demonstrated a self-powered acceleration sensor based on liquid metal TENG with an inner mercury droplet and an outer acrylic shell for vibration measurement and analysis in real time. An electrospinning method was utilized to fabricate the nanofiber-networked PVDF film, which was beneficial to enhance the output of TENG. The relationship between the electric output properties and the vibration acceleration was systematically investigated. The output voltage and current exhibit a good linear relationship with the external acceleration. The acceleration sensor shows good performance with the detection range from 0 to 60 m/s^2 and sensitivity of 0.26 V·s/m^2. The liquid metal mercury drop could significantly enhance the stability and durability of the acceleration sensor. The output voltage and current show negligible drops after nearly 200,000 cycles. Furthermore, a high-speed camera with a frame rate of 4000 Hz was employed to dynamically monitor the working process of the acceleration sensor. The acceleration sensor was very sensitive to small ambient vibrations, such as machine vibration and table vibration. This work not only demonstrates a self-powered acceleration sensor with high sensitivity and wide detection range but also expands TENG's application in self-powered sensing systems.

EXPERIMENTAL SECTION

Electrospinning. PVDF solution with 20 wt % in acton/*N*,*N*-dimethylacetamide (1/1 w/w) was prepared. The resulting clear and homogeneous solution was charged into a syringe that was subjected to a DC voltage up to −18 kV by DC power supply (HDP20−2.0, Tianjin Huida Electronic Components, China). The syringe was placed in a microsyringe pump (TYD01-02, Lead Fluid, China), and the spinning solution was delivered to the blunt needle tip (20 G) at a flow rate of 0.03 mL min^{-1} at a fixed collection distance of 20 cm between the tip of the syringe and plate collector. The spinning was done under a relative humidity of 30%. The film was dried in a drying oven at 40 °C for 48 h and then heat treated at 150 °C for 2h.

Fabrication of the Acceleration Sensor. A 6 mm-thick acrylic sheet was processed by laser cutting and sculpting (TR-6040) to form the outer shell. Thin copper film was deposited on the surface of the tailored nn-PVDF film and acrylic shell by direct current magnetron sputtering method. Finally, a mercury droplet was added into the pit of the acrylic shell, and the nn-PVDF film was attached onto the acrylic substrate.

Electrical Measurement. The open-circuit voltage was measured by using a Keithley 6514 system electrometer, and the short-circuit current was measured by using an SR570 low noise current amplifier (Stanford Research System).

ASSOCIATED CONTENT

Supporting Information

The Supporting Information is available free of charge on the ACS Publications website at DOI: 10.1021/acsnano.7b03818.

List that ranks materials according to their tendency to gain or lose electrons; process flow for fabricating the self-powered acceleration sensor; schematic diagram of electrospinning process; size distribution of PVDF

DOI: 10.1021/acsnano.7b03818
ACS Nano XXXX, XXX, XXX−XXX

nanofibers; open-circuit voltage and short-circuit current of the acceleration sensor at variable accelerations; stability test of the acceleration sensor (PDF)

Simulation of the potential distribution between the mercury and nn-PVDF film upon contact and separation (AVI)

Simulation of the potential distribution of nn-PVDF film and electrodes at electrostatic induction stage (AVI)

Contact-separation process between the mercury droplet and triboelectric layers captured by a high speed camera with a frame rate of 4000 Hz (AVI)

Acceleration sensor detecting the operating state of an automotive engine (AVI)

Self-powered human gait analysis system based on liquid metal TENG (AVI)

AUTHOR INFORMATION

Corresponding Authors

*E-mail wqyang@swjtu.edu.cn.

*E-mail: zhong.wang@mse.gatech.edu.

ORCID

Weiqing Yang: 0000-0001-8828-9862

Zhong Lin Wang: 0000-0002-5530-0380

Author Contributions

⊥These authors contributed equally to this work.

Notes

The authors declare no competing financial interest.

ACKNOWLEDGMENTS

This work is supported by the National Natural Science Foundation of China (no. 51602265), the Scientific and Technological Projects for Distinguished Young Scholars of Sichuan Province (no. 2015JQ0013), China Postdoctoral Science Foundation (no. 2016M592692), the Fundamental Research Funds for the Central Universities of China (no. A0920502051619-72), the Independent Research Project of State Key Laboratory of Traction Power (nos. 2017TPL_Z04 and 2016TPL_Z03), and the Chinese "thousands talents" program for pioneer researchers. The high speed camera was provided by Prof. Longquan Chen from Southwest Jiaotong University.

REFERENCES

(1) Pang, Y. K.; Li, X. H.; Chen, M. X.; Han, C. B.; Zhang, C.; Wang, Z. L. Triboelectric Nanogenerators as a Self-Powered 3D Acceleration Sensor. *ACS Appl. Mater. Interfaces* **2015**, *7*, 19076−19082.

(2) Gao, Z.; Zhang, D. Design, Analysis and Fabrication of a Multidimensional Acceleration Sensor Based on Fully Decoupled Compliant Parallel Mechanism. *Sens. Actuators, A* **2010**, *163*, 418−427.

(3) Sobocinski, M.; Leinonen, M.; Juuti, J.; Mantyniemi, N.; Jantunen, H. A Co-Fired LTCC-PZT Monomorph Bridge Type Acceleration Sensor. *Sens. Actuators, A* **2014**, *216*, 370−375.

(4) Shen, Z.; Tan, C. Y.; Yao, K.; Zhang, L.; Chen, Y. F. A Miniaturized Wireless Accelerometer with Micromachined Piezoelectric Sensing Element. *Sens. Actuators, A* **2016**, *241*, 113−119.

(5) Roy, A. L.; Sarkar, H.; Dutta, A.; Bhattacharyya, T. K. A High Precision SOI MEMS-CMOS ± 4 g Piezoresistive Accelerometer. *Sens. Actuators, A* **2014**, *210*, 77−85.

(6) Yang, W.; Chen, J.; Jing, Q.; Yang, J.; Wen, X.; Su, Y.; Zhu, G.; Bai, P.; Wang, Z. L. 3D Stack Integrated Triboelectric Nanogenerator for Harvesting Vibration Energy. *Adv. Funct. Mater.* **2014**, *24*, 4090−4096.

(7) Guo, H.; Yeh, M.; Zi, Y.; Wen, Z.; Chen, J.; Liu, G.; Hu, C.; Wang, Z. L. Ultralight Cut-Paper-Based Self-Charging Power Unit for Self-Powered Portable Electronic and Medical Systems. *ACS Nano* **2017**, *11*, 4475−4482.

(8) Yang, W.; Chen, J.; Zhu, G.; Wen, X.; Bai, P.; Su, Y.; Lin, Y.; Wang, Z. L. Harvesting Vibration Energy by a Triple-Cantilever Based Triboelectric Nanogenerator. *Nano Res.* **2013**, *6*, 880−886.

(9) Zhang, L.; Jin, L.; Zhang, B.; Deng, W.; Pan, H.; Tang, J.; Zhu, M.; Yang, W. Multifunctional Triboelectric Nanogenerator Based on Porous Micro-Nickel Foam to Harvest Mechanical Energy. *Nano Energy* **2015**, *16*, 516−523.

(10) Li, S.; Peng, W.; Wang, J.; Lin, L.; Zi, Y.; Zhang, G.; Wang, Z. L. All-Elastomer-Based Triboelectric Nanogenerator as a Keyboard Cover to Harvest Typing Energy. *ACS Nano* **2016**, *10*, 7973−7981.

(11) Chen, J.; Huang, Y.; Zhang, N.; Zou, H.; Liu, R.; Tao, C.; Fan, X.; Wang, Z. L. Micro-Cable Structured Textile for Simultaneously Harvesting Solar and Mechanical Energy. *Nat. Energy* **2016**, *1*, 16138.

(12) Zhang, L.; Zhang, B.; Chen, J.; Jin, L.; Deng, W.; Tang, J.; Zhang, H.; Pan, H.; Zhu, M.; Yang, W.; Wang, Z. L. Lawn Structured Triboelectric Nanogenerators for Scavenging Sweeping Wind Energy on Rooftops. *Adv. Mater.* **2016**, *28*, 1650−1656.

(13) Chen, S.; Gao, C.; Tang, W.; Zhu, H.; Han, Y.; Jiang, Q.; Li, T.; Cao, X.; Wang, Z. L. Self-Powered Cleaning of Air Pollution by Wind Driven Triboelectric Nanogenerator. *Nano Energy* **2015**, *14*, 217−225.

(14) Wang, Z. L. Catch Wave Power in Floating Nets. *Nature* **2017**, *542*, 159−160.

(15) Wen, X.; Yang, W.; Jing, Q.; Wang, Z. L. Harvesting Broadband Kinetic Impact Energy from Mechanical Triggering/Vibration and Water Waves. *ACS Nano* **2014**, *8*, 7405−7412.

(16) Zhao, X. J.; Zhu, G.; Fan, Y. J.; Li, H. Y.; Wang, Z. L. Triboelectric Charging at the Nanostructured Solid/Liquid Interface for Area-Scalable Wave Energy Conversion and Its Use in Corrosion Protection. *ACS Nano* **2015**, *9*, 7671−7677.

(17) Yang, W.; Chen, J.; Zhu, G.; Yang, J.; Bai, P.; Su, Y.; Jing, Q.; Cao, X.; Wang, Z. L. Harvesting Energy from the Natural Vibration of Human Walking. *ACS Nano* **2013**, *7*, 11317−11324.

(18) Jin, L.; Chen, J.; Zhang, B.; Deng, W.; Zhang, L.; Zhang, H.; Huang, X.; Zhu, M.; Yang, W.; Wang, Z. L. A Self-Powered Safety Helmet Based on Hybridized Nanogenerator for Emergency. *ACS Nano* **2016**, *10*, 7874−7881.

(19) Fan, F.; Lin, L.; Zhu, G.; Wu, W.; Zhang, R.; Wang, Z. L. Transparent Triboelectric Nanogenerators and Self-Powered Pressure Sensors Based on Micropatterned Plastic Films. *Nano Lett.* **2012**, *12*, 3109−3114.

(20) Chen, J.; Zhu, G.; Yang, W.; Jing, Q.; Bai, P.; Yang, Y.; Hou, T.; Wang, Z. L. Harmonic-Resonator-Based Triboelectric Nanogenerator as a Sustainable Power Source and a Self-Powered Active Vibration Sensor. *Adv. Mater.* **2013**, *25*, 6094−6099.

(21) Zhang, B.; Chen, J.; Jin, L.; Deng, W.; Zhang, L.; Zhang, H.; Zhu, M.; Yang, W.; Wang, Z. L. Rotating-Disk-Based Hybridized Electromagnetic-Triboelectric Nanogenerator for Sustainably Powering Wireless Traffic Volume Sensors. *ACS Nano* **2016**, *10*, 6241−6247.

(22) Yang, W.; Chen, J.; Wen, X.; Jing, Q.; Yang, J.; Su, Y.; Zhu, G.; Wu, W.; Wang, Z. L. Triboelectrification Based Motion Sensor for Human-Machine Interfacing. *ACS Appl. Mater. Interfaces* **2014**, *6*, 7479−7484.

(23) Wu, Y.; Jing, Q.; Chen, J.; Bai, P.; Bai, J.; Zhu, G.; Su, Y.; Wang, Z. L. A Self-Powered Angle Measurement Sensor Based on Triboelectric Nanogenerator. *Adv. Funct. Mater.* **2015**, *25*, 2166−2174.

(24) Li, Y.; Cheng, G.; Lin, Z.; Yang, J.; Lin, L.; Wang, Z. L. Single-Electrode-Based Rotationary Triboelectric Nanogenerator and Its Applications as Self-Powered Contact Area and Eccentric Angle Sensors. *Nano Energy* **2015**, *11*, 323−332.

(25) Zhu, G.; Yang, W. Q.; Zhang, T.; Jing, Q.; Chen, J.; Zhou, Y. S.; Bai, P.; Wang, Z. L. Self-Powered, Ultrasensitive, Flexible Tactile Sensors Based on Contact Electrification. *Nano Lett.* **2014**, *14*, 3208−3213.

DOI: 10.1021/acsnano.7b03818
ACS Nano XXXX, XXX, XXX−XXX

(26) Hu, K.; Xiong, R.; Guo, H.; Ma, R.; Zhang, S.; Wang, Z. L.; Tsukruk, V. V. Self-Powered Electronic Skin with Biotactile Selectivity. *Adv. Mater.* **2016**, *28*, 3549−3556.

(27) Yang, J.; Chen, J.; Liu, Y.; Yang, W.; Su, Y.; Wang, Z. L. Triboelectrification-Based Organic Film Nanogenerator for Acoustic Energy Harvesting and Self-Powered Active Acoustic Sensing. *ACS Nano* **2014**, *8*, 2649−2657.

(28) Jing, Q.; Zhu, G.; Wu, W.; Bai, P.; Xie, Y.; Han, R. P. S.; Wang, Z. L. Self-Powered Triboelectric Velocity Sensor for Dual-Mode Sensing of Rectified Linear and Rotary Motions. *Nano Energy* **2014**, *10*, 305−312.

(29) Zhang, H.; Yang, Y.; Su, Y.; Chen, J.; Adams, K.; Lee, S.; Hu, C.; Wang, Z. L. Triboelectric Nanogenerator for Harvesting Vibration Energy in Full Space and as Self-Powered Acceleration Sensor. *Adv. Funct. Mater.* **2014**, *24*, 1401−1407.

(30) Kim, H.; Kim, J.; Jun, K.; Kim, J.; Seung, W.; Kwon, O. H.; Park, J.; Kim, S.; Oh, I. Silk Nanofiber-Networked Bio-Triboelectric Generator: Silk Bio-TEG. *Adv. Energy Mater.* **2016**, *6*, 1502329.

(31) Yu, B.; Yu, H.; Wang, H.; Zhang, Q.; Zhu, M. High-Power Triboelectric Nanogenerator Prepared from Electrospun Mats with Spongy Parenchyma-Like Structure. *Nano Energy* **2017**, *34*, 69−75.

(32) Huang, T.; Lu, M.; Yu, H.; Zhang, Q.; Wang, H.; Zhu, M. Enhanced Power Output of a Triboelectric Nanogenerator Composed of Electrospun Nanofiber Mats Doped with Graphene Oxide. *Sci. Rep.* **2015**, *5*, 13942.

(33) Won, D.; Baek, S.; Huh, M.; Kim, H.; Lee, S.; Kim, J. Robust Capacitive Touch Sensor Using Liquid Metal Droplets with Large Dynamic Range. *Sens. Actuators, A* **2017**, *259*, 105−111.

(34) Chen, Y.; Liu, Z.; Zhu, D.; Handschuh-Wang, S.; Liang, S.; Yang, J.; Kong, T.; Zhou, X.; Liu, Y.; Zhou, X. Liquid Metal Droplets with High Elasticity, Mobility and Mechanical Robustness. *Mater. Horiz.* **2017**, *4*, 591.

(35) Saurenbach, F.; Wollmann, D.; Terris, B. D.; Diaz, A. F. Force Microscopy of Ion-Containing Polymer Surfaces: Morphology and Charge Structure. *Langmuir* **1992**, *8*, 1199−1203.

(36) Deng, W.; Zhang, B.; Jin, L.; Chen, Y.; Chu, W.; Zhang, H.; Zhu, M.; Yang, W. Enhanced Performance of ZnO Microballoon Arrays for a Triboelectric Nanogenerator. *Nanotechnology* **2017**, *28*, 135401.

(37) Lin, L.; Wang, S.; Niu, S.; Liu, C.; Xie, Y.; Wang, Z. L. Noncontact Free-Rotating Disk Triboelectric Nanogenerator as a Sustainable Energy Harvester and Self-Powered Mechanical Sensor. *ACS Appl. Mater. Interfaces* **2014**, *6*, 3031−3038.

(38) Wang, S.; Lin, L.; Wang, Z. L. Nanoscale Triboelectric-Effect-Enabled Energy Conversion for Sustainably Powering Portable Electronics. *Nano Lett.* **2012**, *12*, 6339−6346.

DOI: 10.1021/acsnano.7b03818
ACS Nano XXXX, XXX, XXX−XXX